

The Scaling of Exact and Approximate Ginsparg-Wilson Fermions

W. Bietenholz

NORDITA
Blegdamsvej 17
DK-2100 Copenhagen Ø, Denmark

and

I. Hip ¹

Institut für Theoretische Physik
Universität Graz
A-8010 Graz, Austria

Preprint NORDITA-99/10-HE
hep-lat/9902019

We construct a number of lattice fermions, which fulfill the Ginsparg-Wilson relation either exactly or approximately, and test them in the framework of the 2-flavor Schwinger model. We start from explicit approximations within a short range, and study this formulation, as well as its correction to an exact Ginsparg-Wilson fermion by the “overlap formula”. Then we suggest a new method to realize this correction perturbatively, without using the tedious square root operator. In this way we combine many favorable properties: good chiral behavior, small mass renormalization, excellent scaling and rotational invariance, as well as a relatively modest computational effort, which makes such formulations most attractive for QCD.

¹Supported by Fonds zur Förderung der Wissenschaftlichen Forschung in Österreich,
Project P11502-PHY.

1 Introduction

Recently there have been intensive new activities to circumvent the notorious Nielsen-Ninomiya No-Go theorem [1] for chiral fermions on the lattice. That theorem has a rather complicated set of minimal assumptions; we simplify them slightly to the following statement: for an (undoubled) lattice fermion, unitarity, discrete translation invariance, locality and (full) chiral symmetry cannot coexist. To get around this theorem, the breaking of each of these properties has been tried. Examples are (referring to the above order) one-sided lattice Dirac operators, random lattices, SLAC and Rebbi fermions, and finally the Wilson fermion.

The latter breaks the full chiral symmetry in a rather hard way, destroying essential physical properties related to chirality. (By full chiral symmetry we mean the relation $\{D, \gamma_5\} = 0$, where D is the lattice Dirac operator, and the curly bracket denotes the anti-commutator.) The subject of this paper is a recently re-discovered approach to perform such a chiral symmetry breaking in a much softer way, preserving a modified but continuous form of chiral symmetry at finite lattice spacing.

That remnant lattice chiral symmetry transformation has first been written down in Ref. [2]. Its generalized form reads (we use a short-hand notation for the convolutions in coordinate space)

$$\bar{\psi}_x \rightarrow \left(\bar{\psi} (1 + \epsilon [1 - DR] \gamma_5) \right)_x, \quad \psi_x \rightarrow \left((1 + \epsilon [1 - DR] \gamma_5) \psi \right)_x \quad (1.1)$$

where R is a *local* Dirac scalar, i.e. it decays at least exponentially. We now require invariance of the fermionic Lagrangian $\bar{\psi} D \psi$ to $O(\epsilon)$. This amounts to the condition

$$\{D_{x,y}, \gamma_5\} = 2(D\gamma_5 R D)_{x,y}, \quad (1.2)$$

which is known as the Ginsparg-Wilson relation (GWR). The crucial point is that the term R , which describes the chiral symmetry breaking of D^{-1} ,

$$R_{x,y} = \frac{1}{2} \gamma_5 \{D_{x,y}^{-1}, \gamma_5\}, \quad (1.3)$$

is local, which is not the case for Wilson fermions, massive fermions etc. Therefore the pole structure of D^{-1} is not affected by R .

Ginsparg and Wilson pointed out a long time ago that this is a particularly soft way to break chiral symmetry on the lattice [3]. Renewed interest was attracted to this approach especially by Ref. [4]. It was demonstrated that it preserves the triangle anomaly [3], that it avoids additive mass renormalization and mixing of matrix elements [5], and that it reproduces the soft pion theorems [6]. So far we refer to vector theories, but the GWR even serves as a basis for the construction of chiral gauge theories [7]. As further applications, the GWR provides for instance a safe continuum limit of the chiral anomaly [8] and of the spontaneous chiral symmetry breaking [9]. It also opens new perspectives in other fields, like random matrix models [10].

As a general ansatz for a solution of the GWR, we write

$$D^{-1} = D_\chi^{-1} + R, \quad \text{where } \{D_\chi^{-1}, \gamma_5\} = 0. \quad (1.4)$$

Now a suitable operator D_χ — with the correct continuum limit — has to be identified, which is non-trivial even in the free case. If it suffers from doubling, non-unitarity or SLAC type non-locality (finite gaps of the free $D_\chi(p)$, where p is the momentum), then that disease is inherited by D . Hence all these options must be discarded. A way out is, however, a non-locality of the Rebbi type [11], where $D_\chi(p)$ has divergences. This still allows for locality of D .

That is exactly the mechanism which is at work to yield local perfect fermions [3] (lattice fermions without lattice artifacts). Here the term R^{-1} plays a specific rôle: in the block variable renormalization group transformation, which leads asymptotically to a perfect action, it is the kernel between the blocks in a Gaussian transformation term.² Also in the interacting case the perfect fermion is a solution of the GWR, in agreement with the fact that it breaks the chiral symmetry only superficially (in the manifest form of the lattice action), but not with respect to the physical observables [12]. However, the perfect fermion can only be constructed perturbatively or in the classical approximation (fixed point action, FPA) [12, 13, 14]. It turned out that the latter is a solution of the GWR too [4], and its locality is optimized by the choice

$$R_{x,y} = \frac{1}{2}\delta_{x,y}, \quad \{D_{x,y}, \gamma_5\} = (D\gamma_5 D)_{x,y}. \quad (1.5)$$

The use of a FPA, together with the corresponding classically perfect topological charge, guarantees that the index theorem is correctly represented on the lattice [4].

We refer to eq. (1.5) as the “*standard form*” of the GWR. For a resulting FPA, the index theorem has been confirmed numerically in the Schwinger model [15], where the topological charge was also defined in the spirit of the FPA.

Except for the FPA, another GW fermion was discovered by H. Neuberger [16]. The locality of that solution has been established analytically in a smooth gauge background and numerically up to moderate coupling strength in QCD [17].

The relaxation of the full chiral symmetry condition to the GWR allows the fermions to be local, but it has been conjectured that they can still not be “ultralocal” [18]. This means that their couplings may decay exponentially, but they cannot stop at a finite number of lattice spacings, not even in the free case. In fact, this has been demonstrated for the standard form of the GWR [19] and for a more general class of GW kernels R in any dimension $d \geq 2$ [20].

Against this background, we construct in the next Section lattice fermions, which satisfy the GWR at least to a good approximation, but which have couplings only in a short range, so that they can be implemented directly for simulations.³ At the same

²Only the limit $R \rightarrow 0$ (“ δ function blocking”) leads to non-locality.

³There is some conceptual — though not technical — similarity with the papers in Ref. [21].

time, we optimized other essential properties, in particular the scaling behavior and the approximate rotation invariance. We emphasize that the GWR does not guarantee a good quality of those properties. In fact, it has been observed [22, 23] — and it will be confirmed in Section 3 — that the Neuberger fermion does a rather poor job with that respect.

In addition we do our best to keep the computational effort modest. In the framework of the Schwinger model, where our study takes place, we can also simulate very complicated actions. However, we are interested in working out a formulation, which has the potential to be carried on and applied to $d = 4$. All the above properties (in particular excellent chirality and scaling) are also manifest in the FPA for the Schwinger model in Ref. [14], except for the simplicity. That (approximate) FPA involves 123 independent couplings — and all together 429 terms per site. Unfortunately this makes an analogous formulation in $d = 4$ inapplicable. So far, all attempts to construct a useful approximate FPA for QCD got stuck in the fermionic part of the action, hence it is strongly motivated to search for a simplified alternative with similar qualities.

2 Hypercubic approximate Ginsparg-Wilson fermions

To improve the lattice fermion, i.e. to suppress lattice artifacts, we have to include couplings to lattice sites beyond nearest neighbors. However, the systematic extension to various lattice spacings amplifies the number of couplings very rapidly. As an option, which seems to allow for a powerful improvement, but which is still tractable in QCD simulations [24, 25], we focus on the “*hypercube fermion*” (HF), where $\bar{\psi}_x$ is coupled to ψ_y if $|x_\mu - y_\mu| \leq 1$ for $\mu = 1 \dots d$, i.e. we couple all sites inside a d dimensional unit hypercube.

2.1 Free hypercube fermions

For free fermions, perfect actions can be computed analytically [13]. However, they can only be local in the sense that their couplings decay exponentially, in agreement with the conjecture about the absence of ultralocal GW fermions. For practical purposes the parameters in the renormalization group transformation can be tuned so that the decay becomes very fast. This is the case for the parameters corresponding to the standard GWR. There the couplings were truncated to the unit hypercube by means of periodic boundary conditions over three lattice spacings [26]. The resulting *truncated perfect* HF (TP-HF) has strongly improved scaling properties compared to the Wilson fermion. Since the truncation is only a small modification, it also approximates the standard GWR to a good accuracy [18].

To fix our notation, we write the free lattice Dirac operator as

$$D_{x,x+r} = D(r) = \rho_\mu(r)\gamma_\mu + \lambda(r) , \quad (x, r \in \mathbb{Z}^d) , \quad (2.1)$$

	TP-HF	CO-HF	SO-HF
$\rho^{(1)} := \rho_1(1, 0)$	0.30938846	0.30583220	0.334
$\rho^{(2)} := \rho_1(1, 1)$	0.09530577	0.09708390	0.083
$\lambda_0 := \lambda(0, 0)$	1.48954496	1.49090692	1.5
$\lambda_1 := \lambda(1, 0)$	-0.24477248	-0.24771369	-0.25
$\lambda_2 := \lambda(1, 1)$	-0.12761376	-0.12501304	-0.125
\mathcal{V}_{st}	$3.008 \cdot 10^{-4}$	$1.006 \cdot 10^{-4}$	$65.518 \cdot 10^{-4}$

Table 1: *The couplings of free hypercube fermions — truncated perfect, chirally optimized and scaling optimized — and their violations of the standard GWR. Note the constraints $\rho^{(1)} + 2\rho^{(2)} = 1/2$ and $\lambda_0 + 4(\lambda_1 + \lambda_2) = 0$ from the continuum limit and from mass zero, respectively.*

where we assume the sensible symmetries: ρ_μ is odd in the μ direction and even in all other directions, while the Dirac scalar λ is entirely even. In addition ρ_μ is invariant under permutations of the non- μ axes, and λ under any permutation of the axes. Of course D must also have the correct continuum limit, $D(p) = ip_\mu\gamma_\mu + O(p^2)$.

As a measure for the total violation of the free GWR, we sum the squared violations in each site,

$$\begin{aligned}
\mathcal{V} &= \sum_r \left[\sum_{x,y,z} 2D(x)\gamma_5 R(y)D(z)\delta_{r,x+y+z} - \{D(r), \gamma_5\} \right]^2 \\
&= 4 \sum_r \left[\sum_{x,y,z} [\lambda(x)R(y)\lambda(z) - \rho_\mu(x)R(y)\rho_\mu(z)]\delta_{r,x+y+z} - \lambda(r) \right]^2. \quad (2.2)
\end{aligned}$$

For the standard GWR (1.5) this simplifies to

$$\mathcal{V}_{st} = \sum_r \left[\sum_x [\lambda(x)\lambda(r-x) - \rho_\mu(x)\rho_\mu(r-x)] - \lambda(r) \right]^2. \quad (2.3)$$

If we just optimize the couplings so that \mathcal{V}_{st} becomes minimal, then we can still do somewhat better than the TP-HF. For $d = 2$ this can be seen from Table 1, where we denote that “*chirally optimized*” HF as CO-HF. However, the chiral optimization makes the scaling behavior a little worse than it is the case for the TP-HF, see below. On the other hand, if we search for excellent scaling, then we end up with a HF that we call SO-HF (*scaling optimized*), and which is also included in Table 1. Its value for \mathcal{V}_{st} is still small, but clearly larger than in the previous two cases. The TP-HF can therefore be seen as a compromise between the two optimizations with respect to just one property. Note that the couplings are similar in all these three HFs.

Actually the comparison of \mathcal{V}_{st} is not really fair for the SO-HF, because that fermion is not necessarily related to the standard GWR. If we allow for $R_{x,y} = r_0\delta_{x,y}$ (r_0 arbitrary),

then its value \mathcal{V} drops to $18.413 \cdot 10^{-4}$ (for $r_0 = 0.48950632$). If R is generalized further to an even hypercubic form (like λ), we arrive at $\mathcal{V} = 15.977 \cdot 10^{-4}$, but this is still not in the same order of magnitude as the TP-HF and CO-HF.

We can also perform the minimization of the HF couplings for such generalized GW kernels R . However, we have to avoid the trivial minimum at $\lambda = R = 0$ (naive fermion), so we insert another constraint on λ . We require the mapping to $d = 1$ to reproduce the 1d Wilson fermion, $\lambda_1 + 2\lambda_2 = -1/2$ (which is also the case for TP-HF). The minimum is still found in the same vicinity, $\rho^{(2)} = 0.09909187$, $\lambda_2 = -0.13035191$, and $R(0, 0) = 0.50514453$, $R(1, 0) = -0.00141375$, $R(1, 1) = 0.00183004$, which shows that — at least with this extra constraint — the vicinity of the standard GWR plays indeed a special rôle. The violation then amounts to $\mathcal{V} = 0.793 \cdot 10^{-4}$, so we can apparently not proceed to lower orders of magnitude any more.

Hence we return to the form $R_{x,y} = r_0 \delta_{x,y}$. In this case, there is a simple way to illustrate the accuracy of the GWR. For an exact GW fermion, the spectrum lies on the circle in the complex plane with center and radius $1/(2r_0)$ [4]. This holds with or without gauge interaction. Therefore we can just check how close the eigenvalues of the approximate GW fermion are to that circle. This is shown in Fig. 1, which confirms the hierarchy measured from \mathcal{V} . The strongest deviations occur in the arc opposite to zero. This arc corresponds to high momenta and therefore a fine resolution, which is sensitive to small inaccuracies of the GWR.

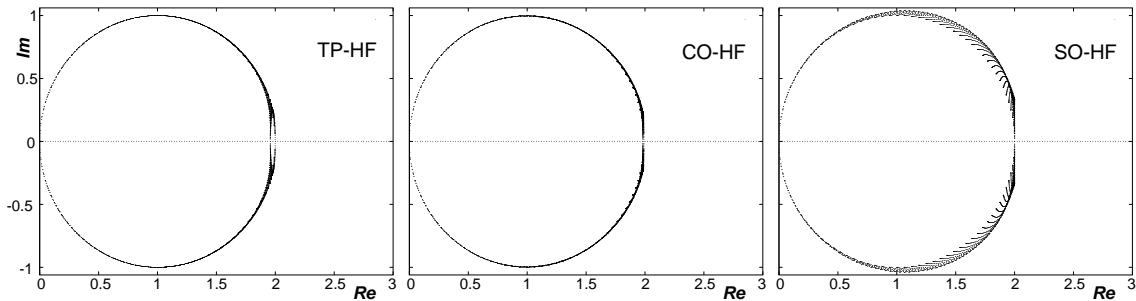


Figure 1: *The free spectra of 3 hypercube fermions: truncated perfect (left), chirally optimized (center) and scaling optimized (right), on a 100×100 lattice.*

However, as we emphasized in the introduction, we do not want to concentrate solely on the chiral quality. In particular we want to consider the scaling behavior as well, and we now take a first look at the impact of such a GWR optimization with that respect. Fig. 2 shows the dispersion relations for the free HF's mentioned before, and we see that all the three are strongly improved compared to the Wilson fermion. We also see that the hierarchy among the HF's is inverted. This observation motivated the consideration of the SO-HF, which was constructed by hand. (Some comments on the construction are given in the appendix.)

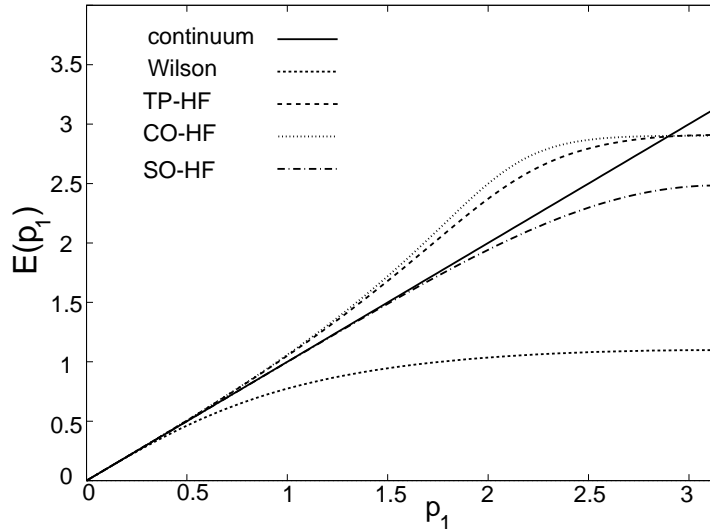


Figure 2: *The dispersion relation for free hypercube fermions compared to the Wilson fermion and to the continuum. (The energies of all higher branches keep above 4.4.)*

We also want to compare thermodynamic scaling properties of the free HFs. In Fig. 3 we show the ratios P/T^2 at $\mu_c = 0$, resp. P/μ_c^2 at $T = 0$, which are scaling quantities in $d = 2$ (P : pressure, T : temperature, μ_c : chemical potential). In the HF actions, μ_c is incorporated according to the prescription in Ref. [27]. For $T \rightarrow 0$ (many lattice points N_t in Euclidean time direction), resp. $\mu_c \rightarrow 0$, all HFs converge to the continuum ratio, but the speed of convergence differs strongly. The relative quality of the scaling behavior, which was suggested by the dispersion, is confirmed. Again the SO-HF looks particularly impressive.

2.2 Applications to the Schwinger model

We now proceed to the 2-flavor Schwinger model (QED₂), and we attach the free fermion couplings equally to the shortest lattice paths only. Moreover we add a clover term, which turned out to be useful, and we fix its coefficient to $c_{SW} = 1$.

The classically perfect fermion-gauge vertex function includes a number of plaquette couplings spread over some range [26]. However, if we sum them up and “compactify” them all into the clover term, we obtain $c_{SW} = 1$. This holds for the “compactified” on-shell $O(a)$ improvement of any of our massless HFs. Note that — unlike QCD — this value does not get renormalized due to the super-renormalizability of the Schwinger model [28]. Therefore, $c_{SW} = 1$ provides a non-perturbative $O(a)$ improvement for the Wilson fermion as well as the HFs.

We use quenched configurations on a 16×16 lattice. However, in the evaluation of dispersion relations and correlation functions (see below) the square of the determinant is included as a weight factor, following the prescription in Ref. [22], Section 3. For the pure

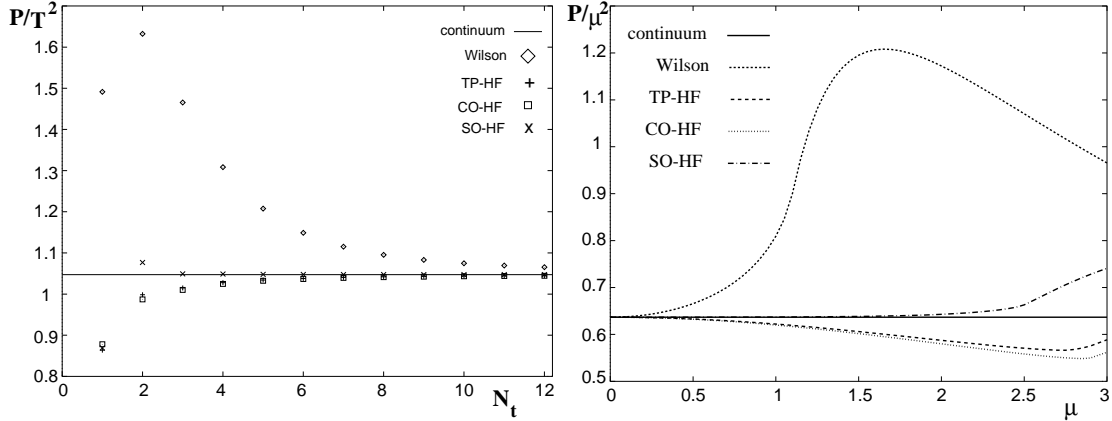


Figure 3: *Thermodynamic scaling ratios. Left: The ratio P/T^2 (at $\mu_c = 0$) as a function of the number N_t of lattice points in the Euclidean time direction. Right: The ratio P/μ_c^2 at $T = 0$ as a function of the chemical potential μ_c .*

gauge part, we use here and throughout this paper the Wilson plaquette action, which is actually perfect in 2d Abelian gauge theory [13].

We first compare the spectra of our three HF at $\beta = 6$. Figs. 4 and 10 show these spectra for a typical configuration. They are still fairly close to the unit circle (SO-HF is closer to a slightly larger circle, in agreement with the observation that it has an optimal $r_0 < 0.5$, see previous subsection). The splitting of the HF spectra around 2 can be viewed as a “residue” of the Wilson double circle. Close to zero we observe that the smallest real eigenvalue becomes finite. In QCD at weak coupling, such an effect corresponds roughly to the quark mass renormalization. Referring to this analogy, we denote the smallest real eigenvalues in the following as “quark” mass renormalization Δm_q . For the HF at $\beta = 6$ it amounts to $\Delta m_q \simeq 0.03$. We also see from Fig. 4 that the clover term has actually a negative impact on the eigenvalues in the region around 2, but it improves the more important eigenvalues close to 0. (In this context, the Sheikholeslami-Wohlert action was studied in the Schwinger model in Ref. [28]; for a systematic study in $d = 4$, see Ref. [29].) In particular it decreases Δm_q , both, for the HF and for the Wilson fermion.⁴ Interestingly the mass renormalization is practically the same for the HF and for the Wilson fermion with clover, and it is again almost the same if we omit the clover term, as it was observed before in QCD [25].

Of course, the mass renormalization — and the deviation from the circle in general — increases at stronger coupling; as an example we show a typical TP-HF spectrum at $\beta = 4$ and at $\beta = 2$ in Fig. 5.

As a scaling test, we consider the dispersion relations of the “mesons”; we call them “ π ” (massless) and “ η ” (massive). In Fig. 6 we show the π and η dispersions for our

⁴Here we refer to the non-critical Wilson fermion: $\rho^{(1)} = -\lambda_1 = 0.5$, $\rho^{(2)} = \lambda_2 = 0$.

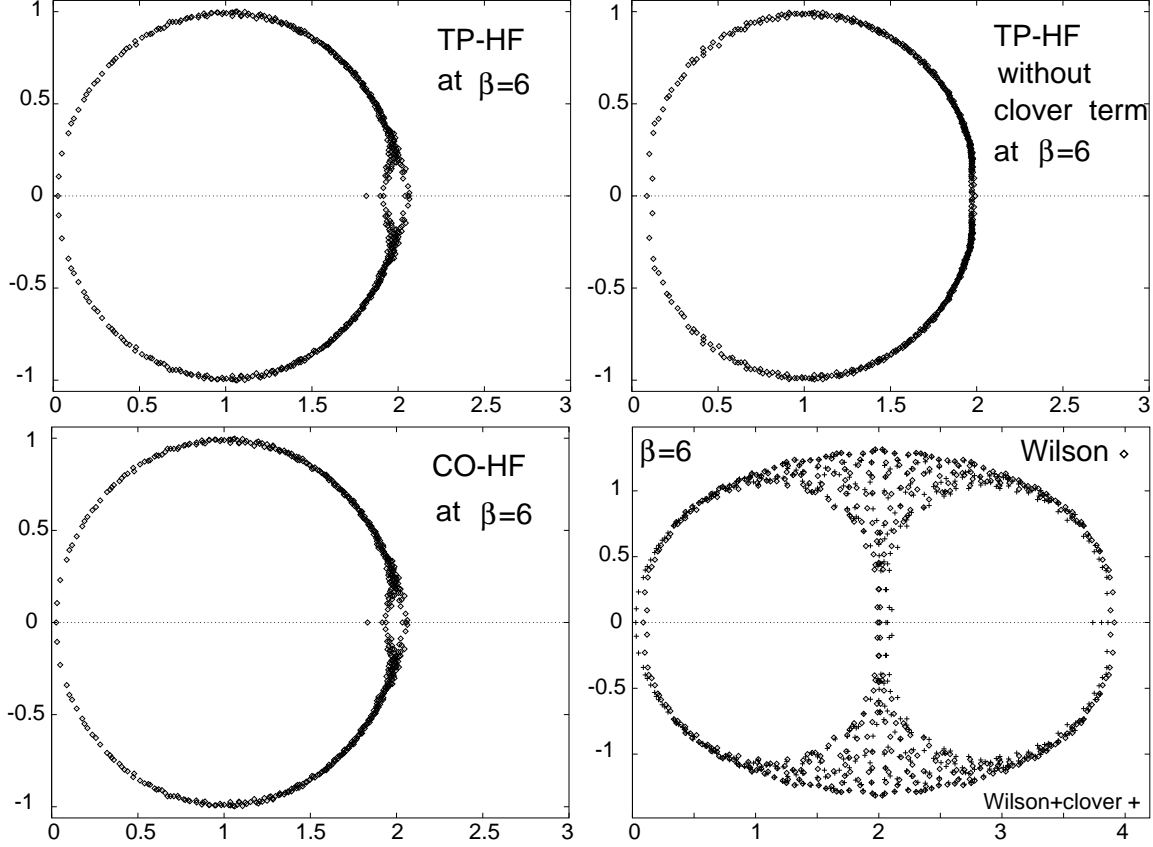


Figure 4: Spectra of different HFs for a typical configuration at $\beta = 6$, compared to the Wilson fermion with and without clover term. (For the SO-HF with the same configuration, see Fig. 10.) The clover term is always included in the HF actions if not stated differently. It has a negative impact in the region around 2, but it improves the more important region close to 0.

three HFs, and we compare them to the results for the Wilson fermion and for the FPA. For the Wilson fermion we now use the critical hopping parameter $\kappa_c = 0.25927$, which was determined using the PCAC relation [30]. These dispersions were obtained from 5000 configurations, using the same ensemble for all the fermion types in Fig. 6 (as well as Fig. 11 in Section 3). We see that our HFs are all strongly improved, to the same level as the FPA. This is very remarkable, because we only use 6 independent terms per site — as opposed to 123 in the FPA. (By contrast, the dispersions for the Sheikholeslami-Wohlert action are very similar to the Wilson action, see first Ref. in [28].) In addition to the excellent scaling — in particular for the SO-HF — the η dispersion also reveals a good agreement with asymptotic scaling, which predicts an η mass of $m_\eta = \sqrt{2/(\pi\beta)} \simeq 0.326$.

As a further test for the quality of our fermion actions, we show in Fig. 7 the decay of

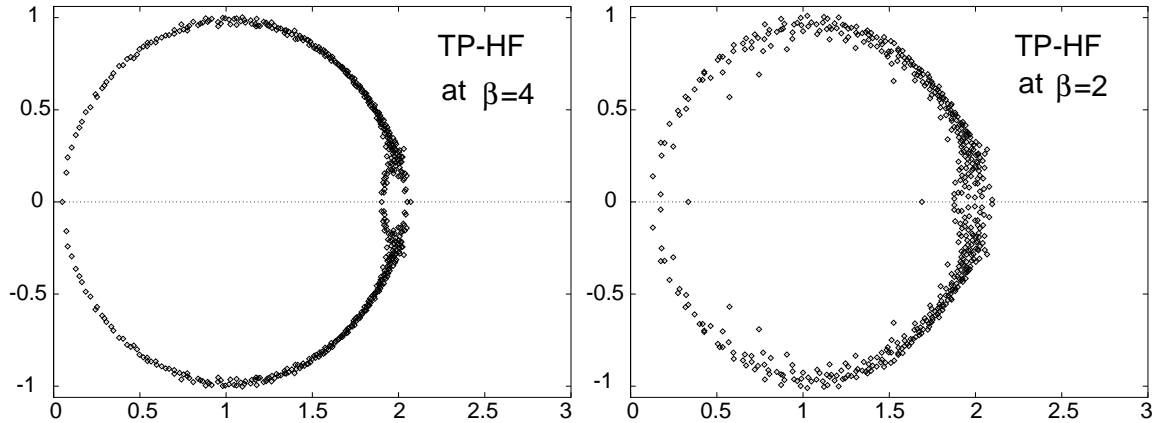


Figure 5: Typical spectra of the TP-HF at $\beta = 4$ and $\beta = 2$. The results for the CO-HF and SO-HF are similar. Strong coupling amplifies the deviation from the unit circle, and in particular the mass renormalization.

the correlation function

$$C_3(x) = \langle \bar{\psi}(0)\sigma_3\psi(0) \cdot \bar{\psi}(x)\sigma_3\psi(x) \rangle. \quad (2.4)$$

We are particularly interested how well rotational invariance is approximated (which can only be measured by using σ_3 [14]). All our HFs yield a very *smooth* decay — again on the same level as the FPA — which reveals an excellent approximation of rotational invariance already at short distances. (The jumps around $|x| \sim 8$ are finite size effects). On the other hand, for the Wilson fermion the decay performs a zigzag at short distances, which corresponds to a “taxi driver metrics”⁵; it takes rather large distances to approximate the Euclidean metrics instead.

Finally we also compared the percentage of configurations, which fulfill the index theorem, if we use the geometric definition for the topological charge. Here the results for the SO-HF are similar to those for the Wilson fermion at $\beta = 6, 4$ and 2 , which were reported in Ref. [22]. The percentages amount to 100 %, 99.5(2) % and 78.7(13) %, respectively.

Our HFs are successful with respect to scaling and rotational invariance, and they approximate the GWR reasonably well up to moderate coupling strength. Their one unpleasant feature is the quite significant mass renormalization, which is visible again in Fig. 6. For the π mass it amounts to $m_\pi \simeq 0.13$ (which is consistent with Δm_q). This is a practical problem: in this formulation, $m_\pi = 0$ would require the tuning of a negative bare mass. For the massive TP-HF that is also unfavorable for locality. However, we do know the TP-HF at any finite bare mass, and we can construct also massive SO-HFs, see

⁵In the “taxi driver metrics”, the distance between two lattice sites is given by the shortest lattice path(s) connecting them.

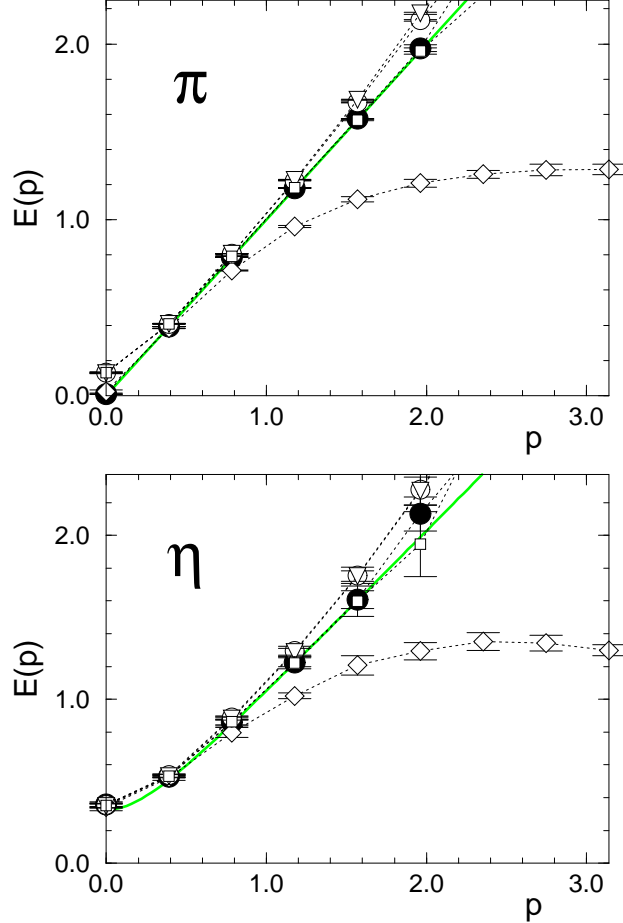


Figure 6: Meson dispersion relations at $\beta = 6$: Wilson fermion (diamonds), TP-HF (empty circles), CO-HF (triangles) and SO-HF (little boxes) — all the HF’s with a clover term — compared to the FPA (filled circles) and the continuum (solid line).

appendix. Here we do not simulate them — that would also contradict our attempt to stay close to the GWR — but in $d = 4$ this option should be reconsidered in order to tackle the problems related to the mass renormalization, which are more difficult there.

Indeed, the same problem was a major obstacle in similar QCD simulations [26, 24, 31, 25]. There the critical bare mass could be shifted to 0 by the use of fat links with *negative* staple terms [32]. We also performed tests with fat links in the present framework, using both, positive and negative staple terms, and we could remove the mass renormalization here too. It is profitable to distinguish a staple term with weight $w_l \lambda_1$ attached to the scalar term, and an independent staple weight $w_r \rho^{(1)}$ attached to the vector term. Then the weight of the direct link is $(1 - 2w_l) \lambda_1$ resp. $(1 - 2w_l) \rho^{(1)}$.⁶ In Table 2 we give results from various staple combinations for the “quark” mass renormalization Δm_q and

⁶An attempt to optimize the fat links analytically — so that the GWR violation is minimized — yielded

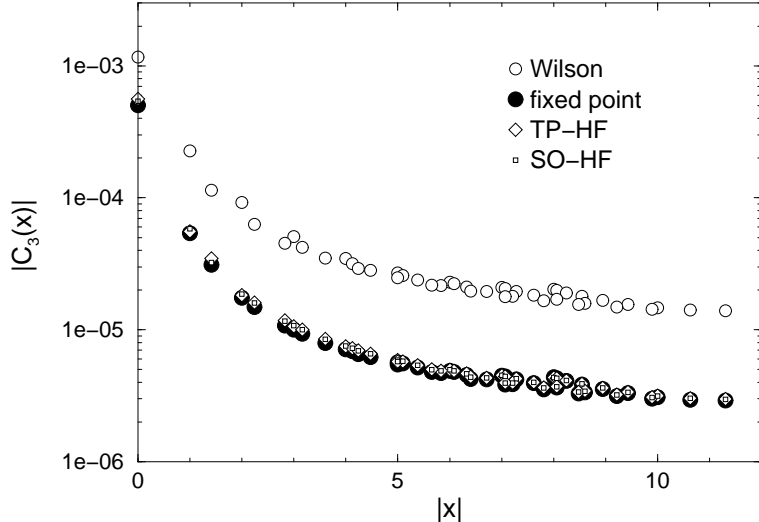


Figure 7: *The decay of the correlation function $|C_3(x)|$ (defined in eq. 2.4), illustrating the level of approximate rotation invariance for various fermion actions.*

for the mean value of the squared distance from the unit circle, $\langle \delta_r^2 \rangle$. The first quantity refers to the (physically essential) small real eigenvalues, and the second quantity to the whole spectrum. In particular, $\Delta m_q = 0$ requires a strongly negative w_l , which amplifies, however, $\langle \delta_r^2 \rangle$. As a remedy for that we can choose a positive w_r (and modify w_l a little). However, here we optimize the GWR only, and it turned out that “GWR optimal” staples are unfavorable for the scaling behavior. The π dispersion relation looks still fine, but the η dispersion is somewhat distorted. For that reason — and for the sake of the simplicity of the action — we do not use fat links in the rest of this paper, i.e. we return to $w_l = w_r = 0$.

Instead, we are going to suggest other solutions for the mass renormalization problem in the following two Sections. The goal is to further reduce the GWR violation, since Δm_q and m_π vanish continuously as \mathcal{V} approaches 0. This is in agreement with the consideration in Ref. [5], where a small fermion mass is introduced as a regularization before taking the chiral limit (in the sense of the GWR).

3 Exactly massless fermions with a good scaling behavior

Let us introduce the operator

$$V = 1 - \frac{1}{\mu} D, \quad (\mu \neq 0) \quad (3.1)$$

positive w_l , w_r , which led, however, to even larger values for Δm_q .

w_l	w_r	Δm_q	$\langle \delta_r^2 \rangle$ (in units of 10^{-3})
0	0	0.032(8)	1.34(4)
0	0.1	0.029(8)	1.07(3)
0	0.2	0.027(7)	0.91(3)
-0.1	0	0.021(6)	1.46(5)
-0.3	0	-0.001(4)	2.07(14)
-0.24	0.2	0.002(4)	1.59(11)

Table 2: Two characteristic quantities to measure the approximation of the standard GWR: the “quark” mass renormalization Δm_q , and the mean value of the squared radial deviations of the eigenvalues from the unit circle (in the complex plane), $\langle \delta_r^2 \rangle$. We show results for varying fat links, with the scalar staple coefficient w_l and the vector staple coefficient w_r , at $\beta = 6$. Criticality can be achieved by a strongly negative w_l .

where μ is a real mass parameter, and we require the GWR to hold with $R_{x,y} = \frac{1}{2\mu}\delta_{x,y}$. This is equivalent to

$$V^{-1} = \gamma_5 V \gamma_5 . \quad (3.2)$$

The overlap type of solution inserts an operator V of the form

$$V = \frac{A}{\sqrt{A^\dagger A}} . \quad (3.3)$$

If this is well-defined, then V is unitary and the GWR reads $V^\dagger = \gamma_5 V \gamma_5$. Inserting some lattice Dirac operator D_0 as

$$A = \mu - D_0 , \quad (3.4)$$

leads to a correctly normalized Dirac operator D . Most of the literature deals with the *Neuberger fermion*, which uses $D_0 = D_W$, where D_W is the Wilson-Dirac operator. Neuberger fermions were simulated (quenched) in the Schwinger model [22, 33, 23] and in 4d non-Abelian gauge theory [34, 17]. The mass parameter μ is usually set to 1. As long as we stay with the Wilson-Dirac operator it can be absorbed in the mass M of D_W . But if we insert a more sophisticated D_0 , then μ takes a non-trivial rôle, see below.

It was observed that the use of a suitable $D_0 = D_{HF}$ instead of D_W improves the locality of the free D significantly [18], and it looks promising also with other respects. Further properties of improved overlap fermions will be discussed in this Section.

3.1 Free overlap fermions

If we insert the ansatz $D_0 = \rho_\mu \gamma_\mu + \lambda$, then the free overlap Dirac operator and its inverse read (in momentum space)

$$\begin{aligned} D(p) &= 1 + \frac{\rho_\mu(p) \gamma_\mu + \lambda(p) - \mu}{\sqrt{-\rho^2(p) + [\lambda(p) - \mu]^2}}, \\ D^{-1}(p) &= \frac{1}{2} \left(1 - \frac{\rho_\mu(p) \gamma_\mu}{Q(p) + u(p)} \right), \quad Q(p) := \sqrt{-\rho^2(p) + u^2(p)}, \quad u(p) := \lambda(p) - \mu. \end{aligned} \quad (3.5)$$

There are two conditions for a pole in the free propagator:

$$(1) \quad \rho^2(p) = 0, \quad (2) \quad u(p) < 0. \quad (3.6)$$

Hence the vector term ρ_μ determines the shape of the fermion dispersion, and the scalar term λ can fix an end-point of that dispersion curve ⁷. (This is different from the usual case, where both terms contribute to the shape, and the curve cannot just end inside the Brillouin zone.) From the symmetry properties that we assumed for the vector term, condition (1) allows for poles whenever all momentum components obey $p_\mu \in \{0, \pi\}$, hence it allows for fermion doubling with 2^d species. However, the condition (2) can still save us from doubling; λ and μ should be chosen such that only the pole at $p = 0$ really occurs. If we insert D_W with a mass M , then the condition for one free species is simply $0 < (\mu - M) < 2$. ⁸ In gauge theory, some tuning of μ might be required to stay with one species [6].

For a HF with an even scalar term λ , the conditions read ⁹

$$\mu - \lambda_0 - 4(\lambda_1 + \lambda_2) > 0, \quad \mu - \lambda_0 + 4\lambda_2 < 0, \quad \mu - \lambda_0 - 8\lambda_2 < 0, \quad (3.7)$$

where we use the notation introduced in Table 1. In the presence of gauge interactions, the 1-species region becomes more narrow from both sides. This can be understood from a crude consideration, which introduces “effective links” somewhat smaller than 1, and which therefore moves the (negative) couplings $\lambda_1 \simeq 2\lambda_2$ to larger “effective” values. This was also observed numerically for the TP-HF in the Schwinger model [35]. ¹⁰ Hence we should start far from the boundaries in the free case, to be on more solid grounds in gauge theory. The truncation by condition (2) should occur not too close to the edge of the Brillouin zone, but of course quite far from $p = 0$, because this region is really needed. It appears that $\mu = 1$ is a very reasonable choice. In Fig. 8 we show the free fermion dispersion for overlap fermion D constructed from D_W and from our three variants of D_{HF} (all of them massless): we show the full curve given by condition (1), and we mark the end-points for $\mu = 1$. Those end-points can be shifted arbitrarily by changing μ . (Higher branches do not appear, see appendix.)

⁷It is the square root which causes this unusual behavior.

⁸The situation *on* the boundaries is tricky.

⁹At this point, we do not insist on $\sum_r \lambda(r) = 0$, i.e. D_{HF} may also be massive.

¹⁰As an example, the massless TP-HF has the free condition is $0 < \mu < 1.96$. At $\beta = 3$ the physical interval shrinks to about $\mu \in (0.3, 1.8)$; outside this interval the index theorem is violated.

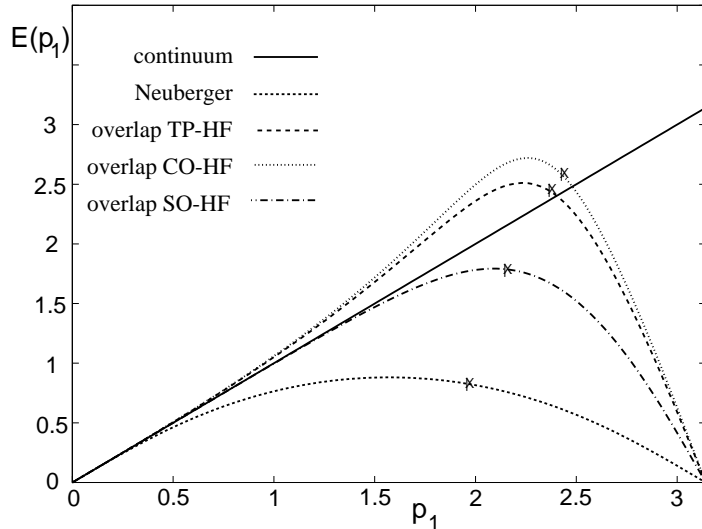


Figure 8: The free dispersion relation for the Neuberger fermion (inserting $D_0 = D_W$ in the overlap formula) and for various improved overlap fermion (inserting $D_0 = D_{HF}$). We mark the end-points of the curves for the mass parameter $\mu = 1$.

We see that the overlap dispersion based on D_W is unfortunately worse than the dispersion of the ordinary Wilson fermion, cf. Fig. 2. (Technically, the reason is that in the ordinary case the scalar term helps to raise the curve a little). It has been conjectured that overlap fermions might be free of $O(a)$ artifacts even in gauge theory. However, for the Neuberger fermion the $O(a^2)$ artifacts are quite bad, as we see even in the free case. The improvement by using D_{HF} is again very significant, in particular for the SO-HF.

The improved scaling of free overlap-HFs is also confirmed if we repeat our thermodynamic considerations, see Fig. 9. The good quality of these fermions does hardly come as a surprise [18]: if we insert a fermion into the overlap formula, which obeys the GWR for $R = \delta_{x,y}/(2\mu)$, then it reproduces itself due to $A^\dagger A = \mu^2$. Now we insert an approximate GW fermion, so its modification by the overlap formula is rather modest, and the good scaling quality does essentially persist.¹¹

In the appendix we comment on the use of massive D_{HF} — which still produce massless overlap fermions — and also on the option to render overlap fermions massive themselves.

3.2 Interacting overlap fermions

Also in the interacting case, the overlap-Dirac operator

$$D = \mu \left[1 - \frac{A}{\sqrt{A^\dagger A}} \right] \quad (3.8)$$

¹¹Here the overlap correction $A \rightarrow \mu A/\sqrt{A^\dagger A}$ is completely obvious.

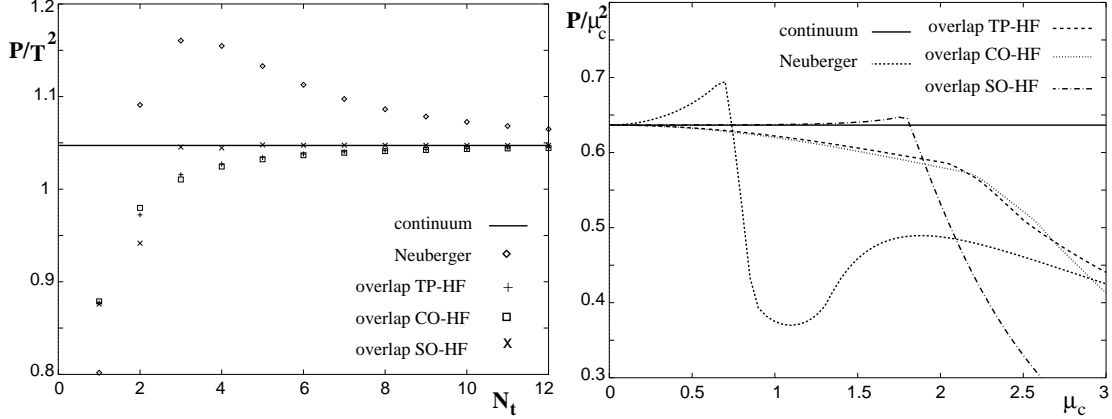


Figure 9: *Thermodynamic scaling ratios: P/T^2 at $\mu_c = 0$ (left), and P/μ_c^2 at $T = 0$ (right), as in Fig. 3, but now for the corresponding overlap fermions. Again the overlap SO-HF is clearly most successful.*

satisfies the GWR with $R_{x,y} = \delta_{x,y}/(2\mu)$, hence its spectrum is situated on the circle with center and radius $1/\mu$. We now wonder what really happens to the eigenvalues of D_{HF} as the hypercube fermion is inserted in the overlap formula. Fig. 10 shows as an example those eigenvalues (for a typical configuration at $\beta = 6$ on our 16×16 lattice) before and after application of the overlap formula. Especially in the region around zero — where the eigenvalue density is low — there is an obvious mapping of the eigenvalues one by one onto the circle. In such cases, the effect of the overlap formula is close to a radial projection of each eigenvalue onto the circle. This can easily be understood from the overlap formula, and it is in agreement with the above statement that the overlap modifies an approximate GW fermion only modestly. (Of course this observation is not so obvious if we insert a fermion far from a GW fermion, such as D_W .)

This geometric understanding of the overlap formula also provides a neat interpretation of the parameter μ : it is simply the center of the circle (through 0) that the spectrum is projected on. Of course that center must be chosen between the small real eigenvalues of the original spectrum (which have to be mapped to 0) and the larger real eigenvalues (to be mapped on 2μ). So the allowed range of μ can be recognized immediately from the spectrum of D_0 , see e.g. Figs. 1, 4, 5 and 10. This range shrinks at stronger coupling. If we do not respect it, then we map one or several eigenvalues to the wrong arc crossing the real axis, and as a consequence the index theorem is violated (as we mentioned already in the previous subsection).

These observations raise hope that also in gauge theory the scaling of an approximate GW fermion is not much affected by the “*chiral projection*”. Indeed, Figs. 11 and 12 show that the scaling quality — tested by the meson dispersion — as well as the approximate rotational invariance is still very good, whereas the Neuberger fermion is contaminated by considerable artifacts (again it is a little worse than the ordinary Wilson fermion). In

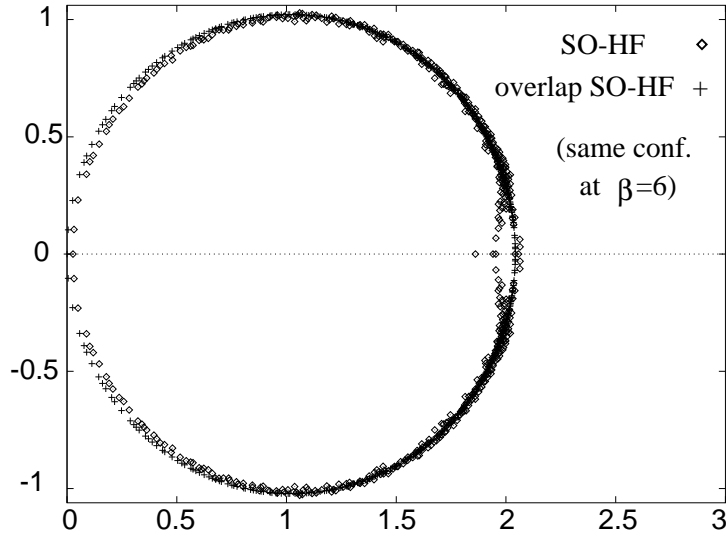


Figure 10: *The mapping of the eigenvalues of the SO-HF (for a configuration at $\beta = 6$) onto the unit circle (in the complex plane) by means of the overlap formula.*

particular for the overlap SO-HF the π dispersion is still excellent, but the η dispersion is a little distorted by the overlap formula (the slope is a bit too steep). The same effect occurs if we remove the mass renormalization by means fat links (using a negative w_l , cf. Section 2.2).

As a further issue, we now want to address the question of locality. For the Neuberger fermion in $d = 4$, locality was established analytically for very smooth gauge fields [17]. At $\mu - M = 1$ the dimensionally generalized condition is that any plaquette variable P has to obey

$$\|1 - P\| < \frac{2}{5d(d-1)}, \quad (3.9)$$

since this rules out the danger of $A^\dagger A = 0$. We see that this condition is more powerful in $d = 2$ than in $d = 4$.

In numerical tests in QCD down to $\beta = 6$, it turned out that the degree of locality is only reduced gradually by the gauge interaction [17].¹² The observation that it remains rather close to the free locality raises hope that the improvement of free locality persists also in gauge theory. In fact, this is confirmed in our Schwinger model study as we see from Fig. 13. It compares first the free locality, and then the absolute value of the maximal correlation over a distance $|x|$ at $\beta = 6$ on a 24×24 lattice. More precisely, we show the

¹²As the interaction is turned on, the value of $\mu - M$, which is optimal for locality, moves somewhat above 1.

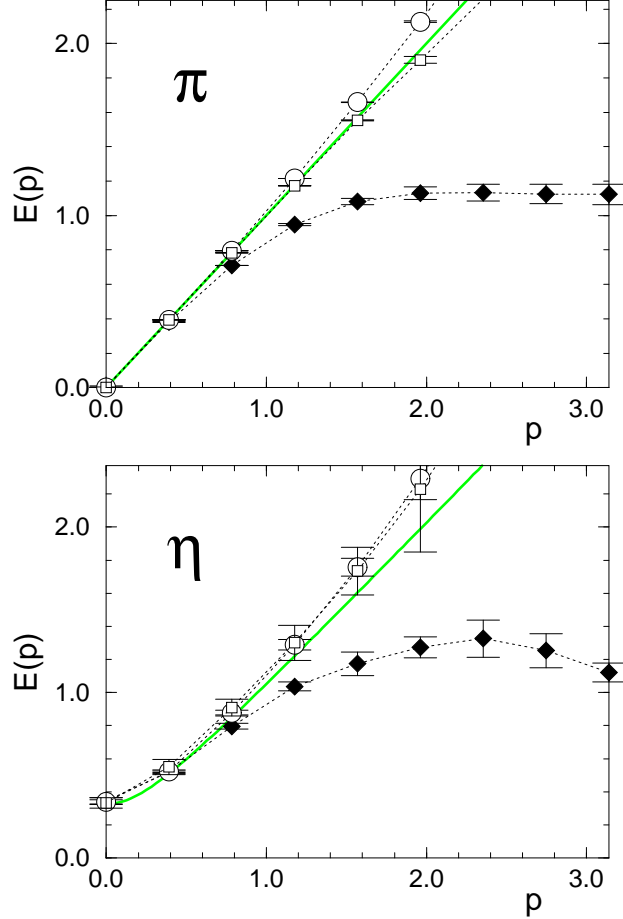


Figure 11: Meson dispersion relations at $\beta = 6$: Neuberger fermion (diamonds), overlap TP-HF (open circles) and the overlap SO-HF (little boxes) compared to the continuum (solid line).

expectation value of

$$\mathbf{f}(\mathbf{r}) = \max_y \{ \|\psi(y)\| \mid |x - y| = \mathbf{r} \} \quad (3.10)$$

for a unit source at x , as it was done before for the Neuberger fermion in QCD [17]. We see that the exponential decay is much faster for the overlap SO-HF than it is the case for the Neuberger fermion. (Again, the little bumps in the middle of that plot are finite size effects; they move continuously if we vary the lattice size.)

A possible danger for the locality of an overlap operator could still occur at strong coupling, if the eigenvalues of $A^\dagger A$ cluster very densely close to zero. Since the use of an exact GW fermion (with respect to $R_{x,y} = \delta_{x,y}/(2\mu)$) for D_0 fixes $A^\dagger A = \mu^2 = \text{const.}$ (for any configuration), one could have hoped that an approximate GW fermion suppresses the density of eigenvalues near zero. However, from the eigenvalue histograms we could not

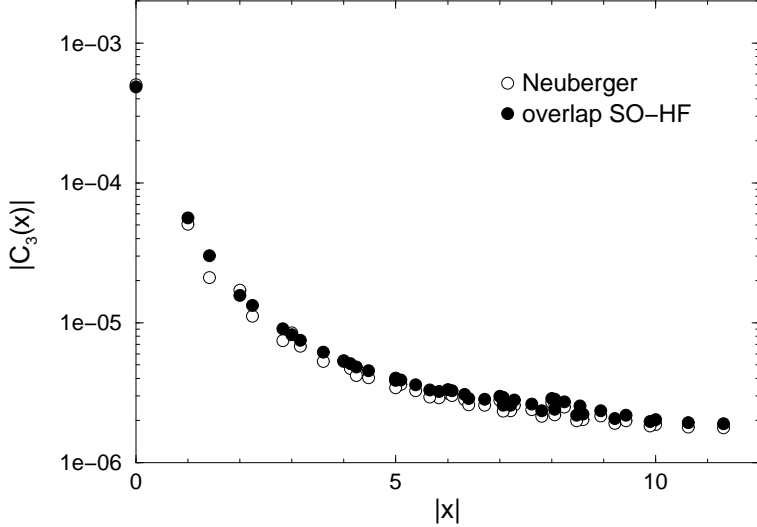


Figure 12: The decay of the correlation function $|C_3(x)|$ (defined in eq. 2.4), illustrating the level of approximate rotation invariance for two overlap fermions.

find any significant difference between the Neuberger fermion and the overlap SO-HF with this respect at $\beta = 6$, and at stronger coupling neither [35]. In Fig. 14 we show histograms of eigenvalues obtained from 1000 configurations at $\beta = 6$: the total eigenvalue density (left) and the lowest two eigenvalues (right). Also if we measure the separation of those lowest two eigenvalues in each configuration, there is no significant difference between the Neuberger fermion and the overlap SO-HF. (Apparently the different degree of locality can be recognized from the small eigenvalue distribution only if one takes into account the (topological) quality of the considered eigenvalues.)

As a last comparison, we show the angular density of the overlap SO-HP and the Neuberger fermion (at $\beta = 6$, using $\mu = 1$) compared to the FPA in Fig. 15.¹³ Since there is a reflection symmetry on the real axis, we only show the upper part, ranging from 0 ($\theta = 0$) to 2 ($\theta = \pi$). At small angles, i.e. small momenta, there is hardly any difference. Again a clear distinction occurs at the opposite arc. The overlap SO-HF has a peak at practically the same angle as the fixed point fermion, in contrast to the Neuberger fermion.

To summarize this Section, we first repeat that the overlap-HFs are exact GW fermions. If they scale very well in the straight application and they approximate the GWR decently — like the SO-HF — then the resulting overlap fermions do still scale well *and* they have an exact remnant chiral symmetry. So they combine two very important properties, which were simultaneously present only in the FPA so far. It's draw-back, however, is that its simulation is still quite involved — although the action is much simpler than the FPA. In $d = 4$ the square root operator is generally problematic, and in addition we use a

¹³For the Neuberger fermion, such an angular density was studied before in Ref. [6].

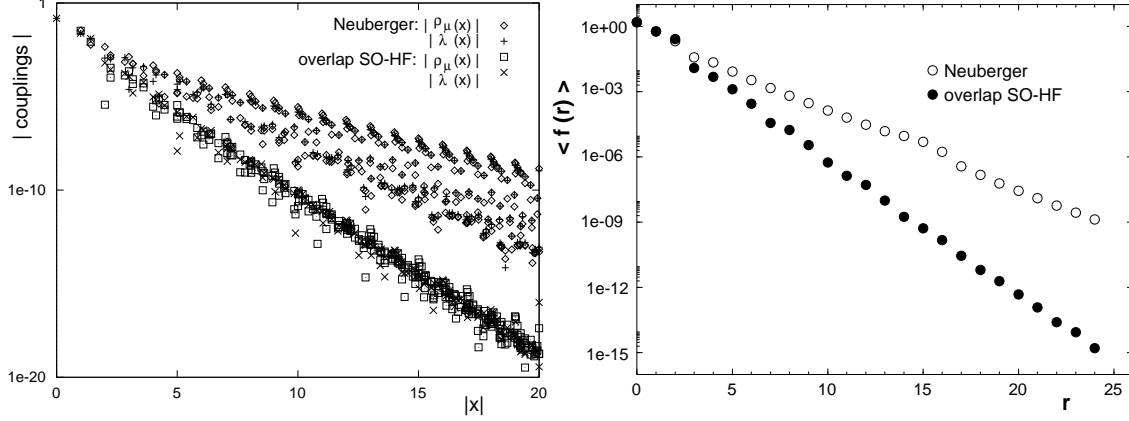


Figure 13: *The locality of the overlap SO-HF compared to the Neuberger fermion. Left: the decay of the free couplings (as introduced in eq. (2.1)). Right: the decay of the maximal correlation (as defined in eq. (3.10)) at $\beta = 6$ on a 24×24 lattice.*

matrix A , which is not as sparse as it is the case for the Neuberger fermion. Therefore the application of such a formulation in QCD might be rather expensive. In the next Section we present a suggestion on how to reduce the computational effort.

4 Perturbative chiral correction

We have seen in Section 2 that suitable HFs can scale well and approximate the GWR reasonably well, up to a certain coupling strength. In Section 3 we converted these HFs into exact GW fermions by means of the overlap formula, without a strong distortion of the good scaling and rotation invariance. However, this formulation contains an inconvenient square root operator. We now suggest a new method to avoid that operator in order to reduce the computational effort. For that purpose, we perform the “chiral projection” perturbatively.

Assume that we start from an operator D_0 , which is close to a GW fermion for $R_{x,y} = \delta_{x,y}/(2\mu)$. Then the operator

$$\varepsilon := A^\dagger A - \mu^2 \quad (4.1)$$

is small, $\|\varepsilon\| \ll 1$, and we use it as an expansion term to approximate $(A^\dagger A)^{-1/2}$. The perturbative chiral projection takes the form

$$\begin{aligned} D_{pcp} &= \mu - AY \\ O(\varepsilon) &: Y = \frac{1}{2} \left[3 - \frac{1}{\mu^2} A^\dagger A \right] \\ O(\varepsilon^2) &: Y = \frac{1}{8} \left[15 - \frac{10}{\mu^2} A^\dagger A + \frac{3}{\mu^4} (A^\dagger A)^2 \right], \quad \text{etc.} \end{aligned} \quad (4.2)$$

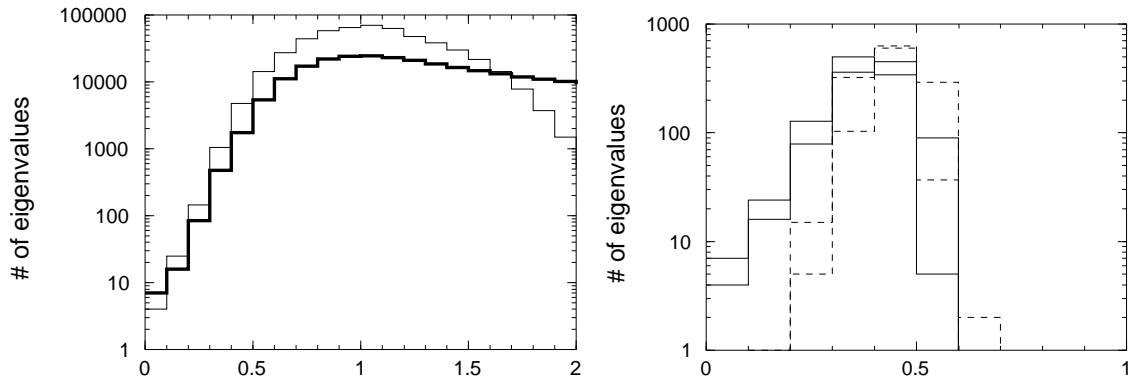


Figure 14: *The eigenvalue distribution of $A^\dagger A$ at $\beta = 6$ for the Neuberger fermion (bold) and the overlap SO-HF (thin) from 1000 configurations. Left: all eigenvalues. Right: the lowest two eigenvalues (solid and dashed).*

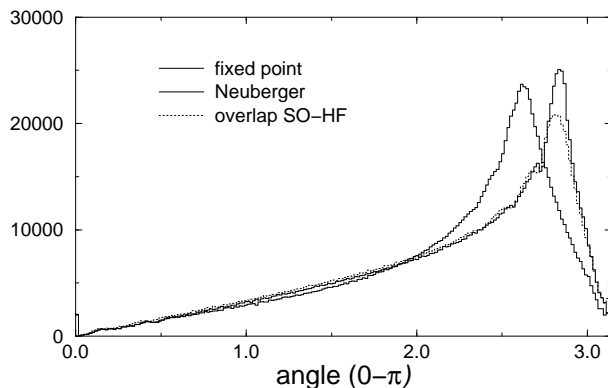


Figure 15: *The angular eigenvalue distribution on the unit circle for various GW fermions, measured in 5000 quenched configurations.*

One could write down the fully explicit action corresponding to the Dirac operator D_{pcp} , but this form is complicated already for $O(\varepsilon)$ (at least the absence of fat links is profitable here). However, for practical applications such an explicit form is not needed, hence we do not write it down here. Once the matrix-vector products Ax and $A^\dagger x$ are implemented, the implementation of the n^{th} order chiral correction is trivial, and requires essentially $1 + 2n$ such multiplications. Taking the first few orders is still much cheaper than the exact chiral projection discussed in Section 3. We emphasize that the linear growth in n is very modest, so it should be feasible to simulate this expansion also beyond the lowest orders.

Let us now discuss the efficiency of the perturbative chiral projection. We consider the SO-HF, which scales very well, but which violates the GWR most (among our HFs). As a first example, we consider the spectrum of the free SO-HF originally and after the first

order chiral projection for $\mu = 1$. Fig. 16 (left) shows that this first order does most of the projection already; the resulting spectrum can hardly be distinguished from the unit circle.

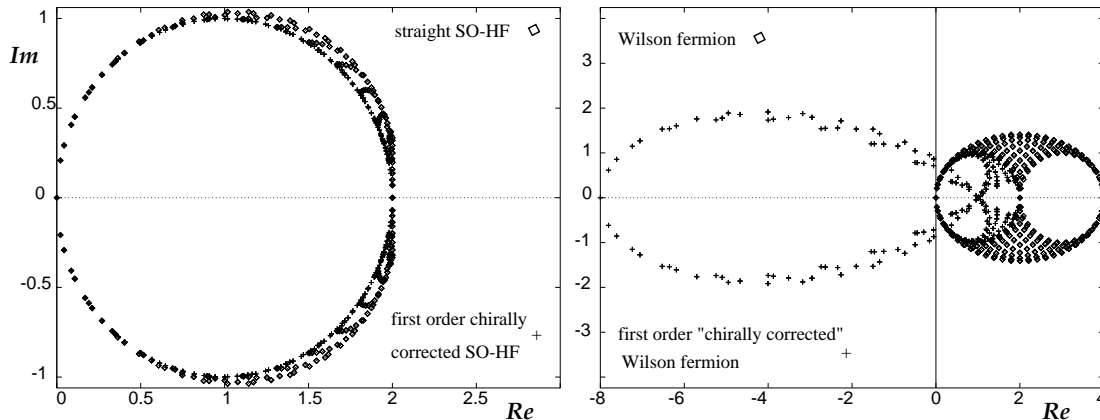


Figure 16: *The initial and the first order chirally corrected free spectrum (using $\mu = 1$) for the SO-HF (left) and for the Wilson fermion (right) on a 30×30 lattice.*

Of course this method only works if we really start from an approximate GW fermion.
¹⁴ As an illustration, we show the spectrum of the free Wilson fermion before and after first order “chiral projection” in Fig. 16 (right). Many eigenvalues do cluster at the unit circle (those corresponding to small eigenvalues of ε), but others diverge in this inadequate expansion (those corresponding to eigenvalues of ε with absolute values > 1). However, for even orders the “tail of the comet” flips far to the right-hand side, and perhaps it does not disturb for practical purposes.

We proceed to the Schwinger model, and we observe that — for our HFs at $\beta = 6$ — the first order chiral correction does almost the full projection already. As an example we consider the SO-HF. Its initial and fully projected spectrum was shown for a typical configuration at $\beta = 6$ in Fig. 10. We now show the first order mapping of the same configuration to the unit circle, and to the closest circle (of radius 1.02145) in Fig. 17 (left). The radius of the larger circle corresponds to the optimal value of r_0 , which was identified in Section 2.1. We observe in particular that the additive “quark” mass renormalization is pressed down from $\Delta m_q \simeq 0.032$ to about 0.014 (and to 0.002 for the second order), which corresponds to a reduction of m_π from 0.13 to 0.07 (resp. 0.02). That effect is specifically illustrated in Fig. 17 (right), which shows the distribution of the small real eigenvalues of 5000 configurations initially and after the perturbative chiral correction to the first and to the second order.

From Fig. 18 (left) we see that at $\beta = 4$ the first order correction is still efficient, and

¹⁴Although simple, the expansion of the square root has not been used before, since all previous overlap simulations used the Neuberger fermion.

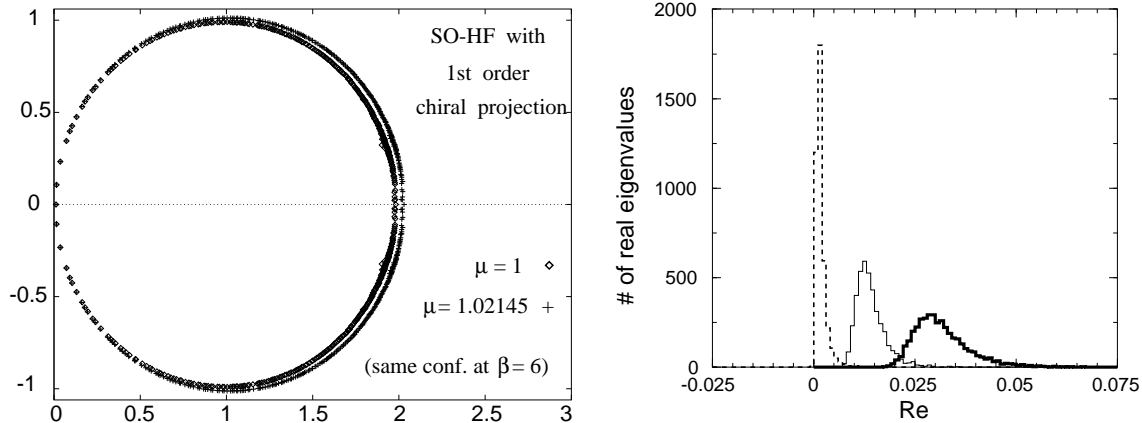


Figure 17: *Left: The spectrum of the first order chirally corrected SO-HF for a configuration at $\beta = 6$ using $\mu = 1$ (smaller circle) resp. $\mu = 1.02145$ (larger circle). Right: A histogram for the small, real eigenvalues of the SO-HF in 5000 quenched configurations at $\beta = 6$: initial (bold), first order chiral correction using $\mu = 1.02145$ (solid) and the corresponding second order correction (dashed). The corrections move the peak — and hence the mass renormalization Δm_q — drastically towards zero (see also Table 3).*

finally Fig. 18 (right) shows that the second order can handle even strong coupling ($\beta = 2$) quite successfully. To quantify these observations we present again the characteristic parameters Δm_q and $\langle \delta_r^2 \rangle$, which were introduced in Section 2.2, see Table 3.

We have seen in Section 3 that the scaling and the approximate rotation invariance are not badly affected by the full chiral projection. In further tests we made the very plausible observation that the effect of a partial chiral projection is in between. It corresponds roughly to the same interpolation as we just observed in the spectrum. Since the chiral behavior can be controlled by this economic method, we would recommend its use most of all for the SO-HF, which provides very good scaling from the beginning.

5 Conclusions

Over the last year, the Ginsparg-Wilson relation became fashionable in the lattice community; about 40 papers have been written about it. However, most of the literature focuses on the chiral properties (and recently on algorithmic questions for the Neuberger fermion [37, 34]) only. Here we discussed chirality together with other crucial properties of fermionic lattice actions, in particular the quality of the scaling behavior, the approximate rotation invariance, the locality and — last but not least — computational simplicity.

We presented three different approaches:

- In Section 2 we discussed the straight construction of approximate GW fermions inside a short range. A few couplings allow for a decent approximation. Such

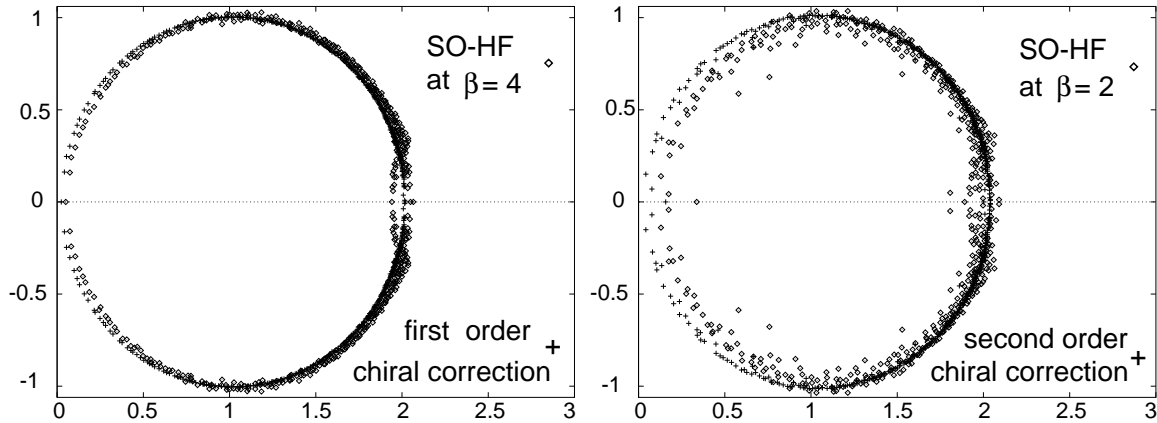


Figure 18: *The spectra the SO-HF initially and after perturbative chiral correction (using $\mu = 1.02145$): $\beta = 4$ and first order correction (left); $\beta = 2$ and second order correction (right).*

fermions are numerically tractable in QCD, and in the Schwinger model we observe good scaling behavior. However, at increasing coupling the GWR violation becomes worse, which is manifest e.g. in a stronger mass renormalization.

- In Section 3 we corrected the GWR in the approximations of Section 2 by means of the overlap formula. We still observe good scaling and approximate rotation invariance for the *improved overlap fermions*, in contrast to the usual Neuberger fermion. However, this formulation is already somewhat demanding, and it is expensive to apply it in $d = 4$.
- In Section 4 we show a way to simplify the evaluation of the overlap action, by avoiding the tedious square root operator. If we start from an approximate GW fermion, then the square root can be replaced by a simple perturbative expansion, and the first one or two orders are computationally relatively cheap. They do, however, provide most of the chiral projection, i.e. the GWR violation becomes small up to a considerable coupling strength. At the same time, scaling and rotation invariance remain strongly improved, in particular for the “scaling optimized hypercube fermion” SO-HF, which appears therefore as most satisfactory.

Based on these results, we think that an extension of this study to $d = 4$ is highly motivated. Regarding the free fermion, all our results are already relevant for $d = 4$ too, because they correspond to the special case $p_3 = p_4 = 0$. An issue in 4d gauge theory is for instance the choice of a suitable action for the pure gauge part.

Acknowledgment *We are indebted to S. Chandrasekharan, who contributed to this work in an early stage. We thank him also for sharing with us his interesting ideas.*

order of the chiral correction	β	Δm_q	$\langle \delta_r^2 \rangle$ (in units of 10^{-3})
0	∞ (free)	0	0.444
1	∞	0	0.000939
2	∞	0	0.00000305
0	6	0.032(8)	0.48(5)
1	6	0.014(4)	0.21(4)
2	6	0.002(2)	0.0015(19)
0	4	0.066(67)	0.89(24)
1	4	0.036(58)	0.52(19)
2	4	0.0014(53)	0.02(12)
0	2	0.31(22)	5.9(20)
1	2	0.23(21)	4.4(17)
2	2	0.17(21)	1.3(11)
∞	any	0	0

Table 3: Two characteristic quantities to measure the approximation of the standard GWR: the “quark” mass renormalization Δm_q , and the mean value of the squared radial deviations of the eigenvalues from the unit circle (in the complex plane), $\langle \delta_r^2 \rangle$ (as in Table 2). We show results for the SO-HF with chiral corrections using $\mu = 1.02145$.

Furthermore we are very thankful to C. B. Lang for many important explanations. We also thank T. DeGrand, Ph. de Forcrand, F. Farchioni, M. Lüscher, K. Orginos T. Pany and K. Splittorff for inspiring comments. I. H. gratefully acknowledges his support by the Fonds zur Förderung der Wissenschaftlichen Forschung in Österreich, Project P11502-PHY, and W. B. thanks for the kind hospitality during his visit to Graz University, where this work picked up its crucial momentum.

A Improved overlap fermions with and without mass

We start this appendix by adding some more details about the (massless) overlap fermions constructed from a hypercube fermion $D_{HF} = \rho_\mu \gamma_\mu + \lambda$. If we replace the momentum component p_2 by $-iE$, then condition (1) in (3.6) yields the free dispersion relation

$$\cosh E = \frac{2\rho^{(1)}\rho^{(2)}f(p_1) \pm \sqrt{1 + [\rho^{(1)2} - 4\rho^{(2)2}]f(p_1)}}{1 - 4\rho^{(2)2}f(p_1)}, \quad \text{with}$$

$$f(p_1) := \left(\frac{\sin p_1}{\rho^{(1)} + 2\rho^{(2)} \cos p_1} \right)^2. \quad (\text{A.1})$$

In all the cases considered in Section 3.1 the lower sign does not lead to a real energy E , hence there are no upper branches.¹⁵ According to condition (2) this curve stops as soon as

$$\lambda_0 + 2\lambda_1(\cos p_1 + \cosh E) + 4\lambda_2 \cos p_1 \cosh E \geq \mu . \quad (\text{A.2})$$

For D_W with mass M , this simplifies to $\cosh E = \sqrt{1 + \sin^2 p_1}$, ending at $\cos p_1 + \sqrt{1 + \sin^2 p_1} \geq 2 + M - \mu$. We observed in Section 3 that the choice $\mu \approx 1$ sets the end-point to a useful position (for $M = 0$).

Taking into account the normalization, the shape of the curve depends on one single parameter, say $\rho^{(2)}$. In the center of the Brillouin zone, the curve rises monotonously with $\rho^{(2)}$, and a good interpolation between D_W ($\rho^{(2)} = 0$) and D_{TP-HF} ($\rho^{(2)} = 0.0953$) makes it practically coincide with the continuum dispersion up to $p_1 \simeq \pi/2$. In this way, the SO-HF was constructed, with a scalar term close to our other two HF's. We saw that it scales excellently, also in the straight application (without overlap).

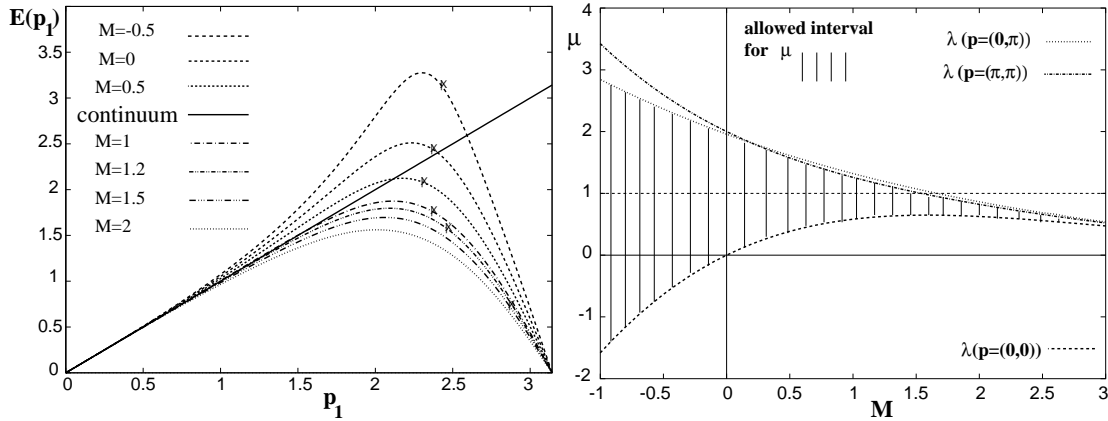


Figure 19: *Left: The free dispersion relation for overlap fermions constructed from massive TP-HFs (with mass parameter M). Again we mark the end-points for $\mu = 1$. Right: The allowed region for μ to provide one flavor for overlap TP-HFs, depending on M .*

Nothing prevents us from also *inserting massive HF's in the overlap formula*; we still obtain massless GW fermions. As an example, we use the massive TP-HF [26], where the parameter M is the mass of the continuum fermion, which was originally blocked to the lattice.¹⁶ If we vary M , the dispersion curve of the overlap fermion can again be deformed monotonously, and a value close to $M = 1$ appears optimal, see Fig. 19 (left). The overlap fermion constructed from the TP-HF at $M \approx 1$ performs also very well in the thermodynamic tests described in Sections 2 and 3, on the same level as the SO-HF. However, in this region of M the 1-species range of the mass parameter μ — introduced

¹⁵Also in all further free dispersions in this appendix, the unphysical sign never yields a real energy.

¹⁶For the TP-HF this implies a bare mass of $M^2/(\exp(M) - 1)$.

in Section 3 — is very narrow, as we see from Fig. 19 (right).¹⁷ Since this is dangerous for the interacting case, we consider the SO-HF as a better approach.

Finally we add some remarks on the case, where an overlap fermion is made massive by adding a mass term at the end. Such massive fermions are likely to have still very good chiral properties, which is useful for simulations of heavy quarks.

We add the mass term in the straightforward manner,¹⁸

$$D_m = 1 + m + \frac{A}{\sqrt{A^\dagger A}} . \quad (\text{A.3})$$

If we now search for poles in the free $D^{-1}(p)$, then condition (1) is generalized compared to (3.6),

$$(1) \quad \rho^2 = \bar{m} (\lambda - \mu)^2 , \quad \bar{m} := 1 - \frac{4}{(1 + m + \frac{1}{1+m})^2} , \quad (\text{A.4})$$

while condition (2) keeps the same form. In Fig. 20 (left) we show the free dispersion relations for various massive overlap fermions. (We now omit the CO-HF; its scaling is always slightly worse than the TP-HF.) They are all constructed by using a massless D_0 and adding $m = 1$. We see that the overlap SO-HF is still good here, but not optimal any more. If we increase $\rho^{(2)}$ a little to 0.088, then we obtain the SOM-HF, which scales excellently in this case.¹⁹ There is no reason for the optimal value of $\rho^{(2)}$ not to depend on m .

The low momentum expansion of the massive overlap operator starts with

$$\begin{aligned} D_m(p) &= m_0 + \frac{1}{2m_{kin}} p^2 + O(p^4) , \\ m_0 &= \text{arcosh} \frac{1}{\sqrt{1 - \bar{m}}} , \\ m_{kin} &= \frac{\sqrt{\bar{m}}}{4} \left(\rho^{(1)2} - \rho^{(2)} + \frac{8\rho^{(1)}\rho^{(2)} + \bar{m}\lambda_1}{2\sqrt{1 - \bar{m}}} + \frac{\rho^{(2)} + 4\rho^{(2)2} + \bar{m}\lambda_2}{1 - \bar{m}} \right)^{-1} . \end{aligned} \quad (\text{A.5})$$

This confirms for instance the value $m_0(m = 1) \simeq 0.693$ for all the massless fermions considered in Fig. 20. In Fig. 21 (left) we plot the static vs. kinetic mass for various overlap fermions, and we see again that the overlap SO-HF performs well at small m_0 . If

¹⁷The asymmetry with respect to the sign of M arises from the kernel in the Gaussian blocking term. We obtain optimal locality for $R_{x,y}^{-1}(M) = \pm \delta_{x,y} M^2 / (\exp(M) - M - 1)$. Above we have chosen the positive sign. Then the couplings of the TP-HF at $M = 1$ are: $\rho^{(1)} = 0.11163921$, $\rho^{(2)} = 0.02885462$, $\lambda_0 = 1.10520159$, $\lambda_1 = -0.09226400$, $\lambda_2 = -0.03854222$. For the negative sign in R^{-1} : $\lambda_i \rightarrow -\lambda_i$.

¹⁸T.-W. Chiu suggested an alternative way [36]. In the notation of Section 1 it amounts to $D'_m = (D_\chi + \bar{m}) / (1 + R D_\chi)$. However, if $R_{x,y} \propto \delta_{x,y}$ then this is equivalent to eq. (A.3), due to $D_m = (1 + Rm) D'_m$, if $\bar{m} = m / (1 + Rm)$, as S. Chandrasekharan first noticed [35].

¹⁹For completeness we give the full set of couplings of the SOM-HF: $\rho^{(1)} = 0.324$, $\rho^{(2)} = 0.088$; $\lambda_0 = 1.5$, $\lambda_1 = -0.25$, $\lambda_2 = -0.125$.

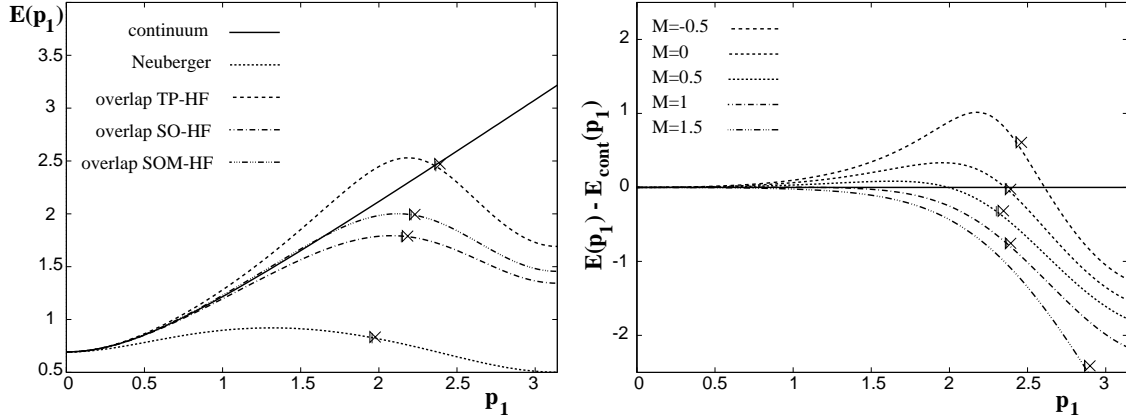


Figure 20: *Left: The free dispersion relation for massive overlap fermions constructed from D_W or from massless HFs. Right: The free dispersion relation for massive overlap fermions constructed from massive HFs. In both plots we mark again the end-points for $\mu = 1$, as a useful example.*

m is of order 1, however, the two masses agree better for the overlap SOM-HF. In a next step, we fix the λ term of the SO-HF ($\lambda_1 = 2\lambda_2 = -1/4$), and we tune the remaining free parameter $\rho^{(2)}$ to an “ideal value”, so that $m_{kin} = m_0$. The resulting $\rho_{ideal}^{(2)}(m_0)$ is shown in Fig. 21 (right). It reveals a smooth mass dependence of the scaling optimal overlap HF.²⁰

Finally we remark that we can also insert a massive D_0 , and make the resulting overlap fermion massive again. As an example, we consider some massive TP-HFs with varying mass parameters M , which are all converted to a massive overlap fermion by adding $m = 1$. Here the static masses m_0 come out differently depending on M . For a direct comparison we show in Fig. 20 (right) the difference between the energy $E(p_1)$ and the continuum energy $E_{cont}(p_1)$. Again the vicinity of $M = 1$ looks very good, but — as we mentioned before — that fermion might be too close to zero- or multi-species (doubling) to be useful in gauge theory.

References

- [1] H. B. Nielsen and M. Ninomiya, Phys. Lett. B105 (1981) 219; Nucl. Phys. B185 (1981) 20 [Erratum: B195 (1982) 541].
- [2] M. Lüscher, Phys. Lett. B428 (1998) 342.
- [3] P. Ginsparg and K. Wilson, Phys. Rev. D25 (1982) 2649.

²⁰Our value for $\rho^{(2)}$ in the SOM-HF is a little larger than $\rho_{ideal}^{(2)}(0.693)$, because this helps the dispersion to follow the continuum curve closely up to larger momenta.

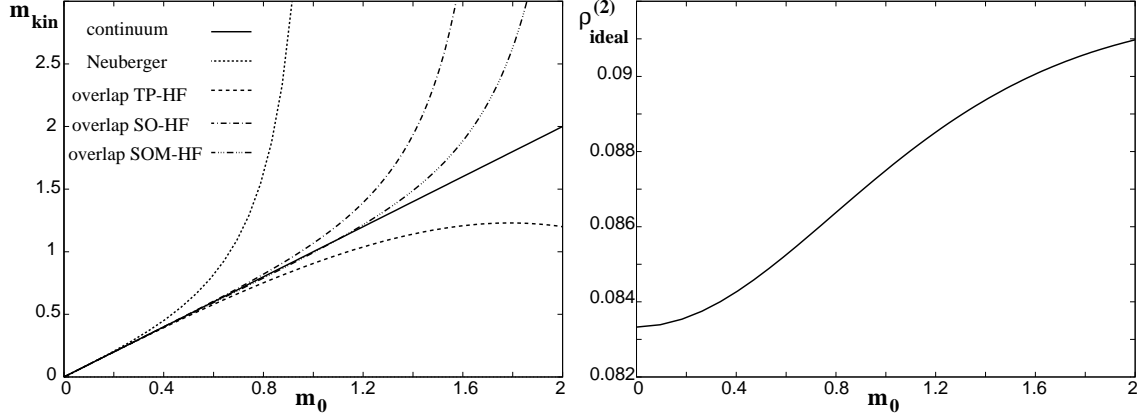


Figure 21: *Left: Kinetic mass m_{kin} vs. static mass m_0 for various types of overlap fermions. Right: The coupling $\rho_{ideal}^{(2)}$ in the massive, scaling optimized HF, which provides $m_0 = m_{kin}$ after insertion in the overlap formula.*

- [4] P. Hasenfratz, V. Laliena and F. Niedermayer, Phys. Lett. B427 (1998) 125.
P. Hasenfratz, Lecture presented in Cambridge (UK), Peñiscola and Kyoto, hep-lat/9803027.
- [5] P. Hasenfratz, Nucl. Phys. B525 (1998) 401.
- [6] S. Chandrasekharan, Phys. Rev. D60 (1999) 074503.
- [7] M. Lüscher, Nucl. Phys. B538 (1999) 515; Nucl. Phys. B549 (1999) 295; hep-lat/9904009.
H. Suzuki, Prog. Theoer. Phys. 101 (1999) 1147.
- [8] K. Fujikawa, Nucl. Phys. B546 (1999) 480.
H. Suzuki, hep-th/9812019.
D. Adams, hep-lat/9812003.
- [9] Y. Kikukawa and A. Yamada, Nucl. Phys. B547 (1999) 413.
- [10] K. Splittorff and A. Jackson, hep-lat/9805018.
K. Splittorff, Nucl. Phys. B548 (1999) 613.
R. Edwards, U. Heller, J. Kiskis and R. Narayanan, Phys. Rev. Lett. 82 (1999) 4188.
- [11] C. Rebbi, Phys. Lett. B186 (1987) 200.
- [12] W. Bietenholz and U.-J. Wiese, Phys. Lett. B378 (1996) 222; Nucl. Phys. B (Proc. Suppl.) 47 (1996) 575.
W. Bietenholz *in* Proc. of the 31st Ahrenschoop Symposium on the Theory of Elementary Particles (World Scientific, 1998) p. 466 (hep-lat/9802014).

- [13] W. Bietenholz and U.-J. Wiese, Nucl. Phys. B464 (1996) 319.
- [14] C. B. Lang and T. Pany, Nucl. Phys. B513 (1998) 645.
- [15] F. Farchioni and V. Laliena, Phys. Rev. D58 (1998) 054501.
F. Farchioni, C. B. Lang and M. Wohlgenannt, Phys. Lett. B433 (1998) 377.
- [16] H. Neuburger, Phys. Lett. B417 (1998) 141; Phys. Lett. B427 (1998) 353.
- [17] P. Hernández, K. Jansen and M. Lüscher, Nucl. Phys. B552 (1999) 363.
- [18] W. Bietenholz, Eur. Phys. J. C6 (1999) 537.
- [19] I. Horváth, Phys. Rev. Lett. 81 (1998) 4063.
- [20] W. Bietenholz, hep-lat/9901005.
I. Horváth, hep-lat/9901014.
- [21] T. DeGrand, A. Hasenfratz and T. Kovács, hep-lat/9807002, Nucl. Phys. B [Proc. Suppl.] 73 (1999) 903.
A. A. Slavnov, Nucl. Phys. B544 (1999) 759.
- [22] F. Farchioni, I. Hip and C. B. Lang, Phys. Lett. B443 (1998) 214.
- [23] F. Farchioni, I. Hip, C. B. Lang and M. Wohlgenannt, Nucl. Phys. B549 (1999) 364.
- [24] T. DeGrand for the MILC collaboration, Phys. Rev. D58 (1998) 094503.
- [25] W. Bietenholz, N. Eicker, A. Frommer, Th. Lippert, B. Medeke, K. Schilling and G. Weuffen, Comput. Phys. Commun. 119 (1999) 1.
- [26] W. Bietenholz, R. Brower, S. Chandrasekharan and U.-J. Wiese, Nucl. Phys. B (Proc. Suppl.) 53 (1997) 921.
- [27] W. Bietenholz and U.-J. Wiese, Phys. Lett. B426 (1998) 114.
W. Bietenholz, Nucl. Phys. A642 (1998) 275.
- [28] Ch. Hoelbling, C. B. Lang and R. Teppner, hep-lat/9807011, Nucl. Phys. B [Proc. Suppl.] 73 (1999) 936.
- [29] C. R. Gatttringer and I. Hip, Nucl. Phys. B541 (1999) 305.
- [30] I. Hip, C. B. Lang and R. Teppner, Nucl. Phys. B (Proc. Suppl.) 63 (1998) 682.
- [31] K. Orginos et al., Nucl. Phys. B (Proc. Suppl.) 63 (1998) 904.
- [32] N. Eicker, talk presented at LATTICE'98. (There is a write-up of this talk, Nucl. Phys. B [Proc. Suppl.] 73 (1999) 850, but it does not describe the experiments with negative staples.)

- [33] S. Chandrasekharan, Phys. Rev. D59 (1999) 094502.
- [34] R. Edwards, U. Heller and R. Narayanan, Nucl. Phys. B540 (1999) 457, Phys. Rev. D59 (1999) 094510.
- [35] S. Chandrasekharan, private communication.
- [36] T.-W. Chiu, Phys. Rev. D60 (1999) 034503.
- [37] H. Neuberger, Phys. Rev. Lett. 81 (1998) 4060, hep-lat/9811019, hep-lat/9901003.
A. Boriçi, Phys. Lett. B453 (1999) 46.
C. Liu, Nucl. Phys. B554 (1999) 313.